



PCCP

Magnetic structure and internal field nuclear magnetic resonance of cobalt nanowires

Journal:	<i>Physical Chemistry Chemical Physics</i>
Manuscript ID	CP-ART-11-2021-005164.R2
Article Type:	Paper
Date Submitted by the Author:	28-Apr-2022
Complete List of Authors:	Scholzen, Pascal; ESPCI Paris, PSL Research University Lang, Guillaume; CNRS, LPEM UMR CNRS 7615 Andreev, Andrey; TotalEnergies SE, One Tech Belgium Quintana, Alberto; Universitat Autònoma de Barcelona, Physics Malloy, James; Georgetown University, Physics Department Jensen, Christopher; Georgetown University, Physics Department Liu, Kai; Georgetown University, Physics Department d'Espinose de Lacaillerie, Jean-Baptiste; ESPCI Paris, PSL Research University

SCHOLARONE™
Manuscripts

Magnetic structure and internal field nuclear magnetic resonance of cobalt nanowires

Pascal Scholzen,¹ Guillaume Lang,² Andrey S. Andreev,³ Alberto Quintana,^{4†} James Malloy,⁴

Christopher J. Jensen,⁴ Kai Liu,⁴ and Jean-Baptiste d'Espinose de Lacaillerie^{1}*

(1) Soft Matter Science and Engineering, ESPCI Paris, Université PSL, UMR CNRS 7615,
Sorbonne Université, 75005 Paris, France.

(2) Laboratoire de Physique et d'Étude des Matériaux, UMR CNRS 8213, ESPCI Paris,
Université PSL, Sorbonne Université, 75005 Paris, France.

(3) TotalEnergies One Tech Belgium (TEOTB), Zone Industrielle C, 7181 Feluy, Belgium

(4) Physics Department, Georgetown University, Washington, DC 20057, USA

KEYWORDS. ⁵⁹Co NMR, internal field NMR, ferromagnetism, metallic nanostructures,
nanomagnetism, FNR.

ABSTRACT:

The magnetic properties of cobalt metal nanowires grown by electrodeposition in porous membranes depend largely on the synthesis conditions. Here, we focus on the role of electrolyte additives on the magnetic anisotropy of the electrodeposited nanowires. Through magnetometry and internal field nuclear magnetic resonance (IF NMR) studies, we compared both the magnetic and crystalline structures of 50 and 200 nm diameter Co nanowires synthesized in presence or absence of organic additives. The spectral characteristics of IF NMR were compared structurally to x-ray diffraction patterns, and the anisotropy of the NMR enhancement factor in ferromagnetic multidomain structures to magnetometry results. While the magnetic behavior of the 50 nm nanowires was dominated, as expected, by shape anisotropy with magnetic domains oriented on axis, the analysis of the 200 nm proved to be more complex. ^{59}Co IF NMR revealed that the determining difference between the samples electrodeposited in presence or in absence of

organic additives was not the dominant crystalline system (*fcc* or *hcp*) but the coherent domain sizes and boundaries. In the presence of organic additives, the cobalt crystal domains are smaller and with defective grain boundaries, as revealed by resonances below 210 MHz. This prevented the development in the Co *hcp* part of the sample of the strong magnetocrystalline anisotropy that was observed in the absence of organic additives. In the presence of organic additives, even in nanowires as wide as 200 nm, the magnetic behavior remained determined by the shape anisotropy with a positive effective magnetic anisotropy and strong anisotropy of the NMR enhancement factor.

1. INTRODUCTION

Ferromagnetic nanowires with tunable magnetic properties have been the focus of intense research efforts, not only because they raise interesting fundamental physics questions but also because of their technological relevance.^{1,2} For example, they can be used for ultra-high density magnetic recording,³ in magnetic field sensors or random-access memories exploiting the giant

magnetoresistance observed in the case of multilayered nanowires.⁴⁻⁷ Recently, ferromagnetic nanowires have attracted interest in curvature-induced topologically protected magnetization textures,^{8,9} as well as prototype structures for 3D information storage.¹⁰ Electrodeposition is a cost-effective and versatile technique that allows for easy and broad tuning of microstructures by simply adjusting growth parameters or electrolyte recipes.^{11,12} Progress in producing arrays of ferromagnetic materials by electrodeposition into porous membranes made of polycarbonate (PC) or anodized aluminum oxide (AAO) has stimulated research by providing model systems to study the structural and electromagnetic properties of metallic nanowire assemblies.^{10,13-16}

Of particular interest is the issue of domain wall structure and dynamics. In soft magnetic nanowires, magnetic domain walls form perpendicularly to the wire axis and can propagate collectively along the wire under the drive of magnetic fields,¹⁷ spin-polarized currents¹⁸ or electric fields.¹⁹ This property lies at the basis of racetrack memory devices.²⁰ Most studies so far have explored the dynamic and static structures of domains and domain walls by magnetometry,^{10,21,22} pulsed resistometry²³⁻²⁵ and magnetic imaging.^{18,26-29} In this work however, we probed the magnetic structure of arrays of parallel cobalt nanowires by ⁵⁹Co internal field nuclear magnetic resonance (IF NMR), with a particular focus on the domain wall response to

radiofrequency (*rf*) fields. This particular form of solid-state NMR is as old as NMR itself³⁰ but has raised a renewed interest because to its ability to probe cobalt nanoparticles in catalysts or battery materials.^{31–33}

In contrast to diamagnetic/paramagnetic materials, conventional (Zeeman) solid-state NMR is not suited to studying ferromagnetic materials and instead, it is the internal hyperfine field inside these structures that is responsible for lifting the degeneracy of the nuclear spin levels. For the study of (ferromagnetic) cobalt nanowires, internal field (IF) NMR thus represents a well-adapted technique due to the possibility to simultaneously analyze the crystalline and magnetic properties of the samples.

Strijkers et al.³⁴ successfully adopted this approach to determine the crystalline structure and crystal orientation inside cobalt wire samples, as well as the influence of the dipole-dipole interactions on the magnetic structure. For this, they used a combination of experiments at zero field and in the presence of an external field oriented parallel or perpendicular to the wire axis. Others have addressed nanowires made of pure cobalt as well as Co-Cu alloys and multilayers.^{35–}

³⁸ In combination with x-ray diffraction (XRD) measurements, they studied the crystalline structure of those three kinds of samples for different synthesis parameters. They found that a

fast deposition rate favors the appearance of a *fcc* crystalline structure, while a pure *hcp* phase is formed using slow deposition rates.

Nevertheless, in cobalt nanowires, how synthesis conditions determine precisely the magnetic domain structure inside the wires remains an open question. In this paper, we study the magnetic and crystalline structures of cobalt nanowires electrodeposited inside the 50 nm and 200 nm cylindrical pores of PC and AAO membranes, respectively. The samples were studied by IF NMR experiments (without an applied field), supported by XRD, scanning electron microscopy (SEM) and magnetometry as complementary experiments. The first goal was to obtain new information on the crystalline and magnetic structure for nanowires obtained with different electrodeposition conditions, focusing on the influence of additives. Secondly, we wished to exemplify the methodological potential of simple IF NMR experiments in strongly anisotropic ferromagnetic structures, such as nanowires. The NMR spectral features complemented XRD for crystalline phase determination, while the analysis of the anisotropy of the enhancement of the *rf* field revealed the orientation of the magnetic domains inside the nanowires.

2. MATERIALS AND METHODS

Sample Synthesis. All reagents have been used without any further purification: Cobalt sulfate heptahydrate ($\text{CoSO}_4 \cdot 7\text{H}_2\text{O}$ ReagentPlus $\geq 99\%$), Cobalt chloride hexahydrate ($\text{CoCl}_2 \cdot 6\text{H}_2\text{O}$ ACS reagent, 98%), Boric Acid (H_3BO_3 ACS reagent, $\geq 99.5\%$), Polyethylene Glycol (PEG – Mn 20000), 1-(2-Hydroxyethyl)-2-Imidazolidinethione ($\text{C}_5\text{H}_{10}\text{N}_2\text{OS}$), Thioglycolic Acid ($\text{C}_2\text{H}_4\text{O}_2\text{S}$ $\geq 98\%$), Janus Green B (3-Diethylamino-7-(4-dimethylaminophenylazo)-5-phenylphenazinium chloride).

Cobalt nanowires of 50 nm and 200 nm diameter were synthesized by template-assisted electrodeposition using a Princeton Applied Research Potentiostat 263A. For the 50 nm diameter nanowires, $6\mu\text{m}$ thick track-etched polycarbonate membranes (PC) with a pore density of $6 \times 10^8 \text{ cm}^{-2}$ were used,³⁹ after coating with Au back electrodes. For the 200 nm diameter nanowires, $60\mu\text{m}$ thick anodized aluminum oxide (AAO) membranes with a pore density of 10^9 cm^{-2} were used,⁴⁰ after coating with Cu back electrodes.

Electrolytes formulation used in this project were adapted from prior studies.^{5,40,41} For the additive-free electrolyte, a Watts-like⁴² electrolyte with Ni replaced by Co precursors was employed. Specifically, the electrolyte was composed of 240 g/L $\text{CoSO}_4 \cdot 7\text{H}_2\text{O}$ + 50 g/L $\text{CoCl}_2 \cdot 6\text{H}_2\text{O}$ + 40 g/L H_3BO_3 . For the additive-containing electrolyte, the same recipe as the additive-free solution was used, with the addition of a mixture of 60 mg/L PEG + 34 $\mu\text{g/L}$ Janus Green B + 34 $\mu\text{g/L}$ 1-(2-Hydroxyethyl)-2-Imidazolidinethione + 12 $\mu\text{g/L}$ Thioglycolic Acid. In both solutions, pH was left unaltered and neither of the solutions were deaerated nor stirred prior to or during the growth. All samples were grown potentiostatically at -1.1V relative to an

Ag^+/AgCl reference electrode. Deposition time was controlled to avoid overplating. After the synthesis, the Cu back electrodes on the AAO membranes were etched away using 2M FeCl_3 , while the Au electrodes on PC membranes were not removed.

In summary, using the same electrodeposition method for each of the two diameters under consideration, Co nanowires were grown with and without additives resulting in a total of four samples.

SEM. Scanning Electron Microscopy images were obtained on two different microscopes. The two 200 nm AAO samples were imaged on a Magellan 400 (ThermoFisher Scientific, USA) in a high vacuum. The 50 nm PC sample was analyzed on a Quattro ThermoFisher under a 100 Pa water vapor atmosphere, in order to avoid charge accumulation at the sample surface due to the lower cobalt content of the sample. Both instruments were used in secondary electron mode with a Field Emission Gun at a voltage of 5 kV.

XRD. X-ray diffraction was performed using a X'Pert (Philips) diffractometer with a PW3050 ($\theta/2\theta$) goniometer between 35° and 100° and with Cu as the anode material operated at 40 mA, 40 kV. The samples were positioned with the plane of the membrane in the reflection plane of the XRD experiment. As a result, it is mainly the crystallographic planes perpendicular to the wire axis that diffracted, as shown in **Figure 1**, with small deviations expected due to imperfect

alignment of the pores in the membranes. The ICDD reference files for spectra corresponding to *fcc* and *hcp* Co are PDF cards No. 00-015-0806 and 00-005-0727, respectively. Note that the gold electrode remaining on the 50 nm PC sample saturated the signal, masking the cobalt nanowire signal. As a result, no structural analysis of the cobalt by XRD could be performed on this sample.

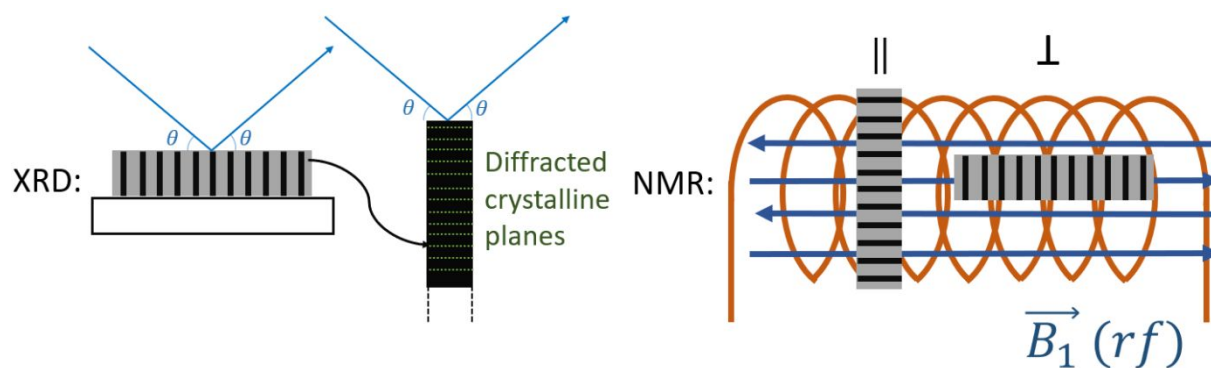


Figure 1. Schematic representation of the XRD and IF NMR experimental geometries. The membrane templates are shown in grey and the cobalt nanowires in black. XRD: The membrane sample was situated in the diffraction plane, i.e., diffraction came mainly from the crystallographic planes parallel to the membrane, or perpendicular to the wire axis. NMR: The samples were tested with two different orientations between the wire axis and the axis of the

excitation and pick-up coil: Parallel (\parallel) and Perpendicular (\perp) to the excitation magnetic field B_1 inside the coil.

⁵⁹Co IF NMR. All NMR experiments were carried out at zero external field, using a SCOUT spectrometer (TECMAG, USA) and a commercial static broadband probe with a 5 mm solenoid excitation/pick-up coil (NMR-Service, Germany). Although the experiments were performed at ambient temperature, the probe was inserted inside a cryostat (Oxford Instruments, UK) for *rf* shielding purposes. The spectra were acquired point-by-point using spin-echo with frequency steps of 0.5 MHz. The spin-echo sequence was composed of two equal *rf* pulses of 1 μ s with an interpulse delay of 8 μ s. The repetition rate of the sequence was 67 Hz, thanks to the very short relaxation time of ferromagnetic cobalt, and the number of transients per point was equal to 4 k. In order to obtain quantitative spectra, the pulse power was varied over 20 dB (i.e., over two orders of magnitude for the *rf* power or one order of magnitude for the *rf* field B_1 amplitude) at each frequency point. The signal from the pulse power giving the maximum signal intensity at each frequency was chosen and used for the spectrum. The lower this power for a certain frequency, the higher the so-called enhancement factor and *vice-versa*. The enhancement factor is defined by the ratio of the excitation field seen by the nuclear spins during an impulsion and

the magnitude of the *rf* field itself and allows to obtain additional information about the cobalt magnetic structure.^{43,44} In order to quantify the pulse power, the peak voltage was measured using an oscilloscope, which allowed to calculate the effective pulse power. The T_2 relaxation time at the main peaks was estimated by varying the interpulse delay and the spectral intensities over the whole spectrum were corrected accordingly as well as for the frequency (ω^2) dependence of the signal intensity. An overview of the measured relaxation times is given in the Supplementary information (Table S3). The corrected spectra were fitted using the DMFIT program.⁴⁵ The peak attribution is described in the upcoming section of this work and more details about the fitting procedure can be found in the Supplementary information (Table S4).

To facilitate their insertion in a glass NMR tube fitting the 5 mm coil, the membranes containing the nanowires were cut into strips. In the case of the 200 nm AAO samples, the quantity of Co inside a single strip was already sufficiently high to obtain a good NMR signal. This was not the case for the 50 nm nanowire samples which have smaller nanowires with a lower density, and for which six of the membrane strips were stacked inside the NMR tube. As the orientation of the excitation field with respect to the wire main axis is crucial, each sample was tested at two different orientations, as shown in Figure 1. Since the nanowires are oriented normal to the

membrane, for the first orientation, called *parallel*, the membranes were put perpendicular to the coil axis. This corresponded to a parallel orientation of the nanowire axis with respect to the excitation field. Similarly, for the *perpendicular* orientation, the membranes were placed parallel to the coil axis.

Magnetic characterization. Magnetic properties of the synthesized samples were studied by vibrating sample magnetometry (VSM) using a Princeton Measurement Corporation MicroMag 3900, as well as a Quantum Design Materials Property Measurement System (MPMS3). Hysteresis loops were measured at room temperature with an external field, up to 1.8 T, applied either parallel or perpendicular to the wire axis.

3. RESULTS

SEM. In order to verify the pore diameter, spacing and regularity, SEM analysis was performed on the samples. As shown in the tilted view of Figure 2a, the 200 nm pores inside the AAO samples were not completely filled with cobalt, in order to avoid overplating. In addition, the upper end of the pores, close to membrane surface, seemed to be quite defaulted due to a

damaged surface, which was without consequence because of their incomplete filling. The AAO membranes, produced by anodic oxidation of aluminum in acidic solution, had interpore separations smaller than the pore diameter. On the other hand, as shown in Figure 2b, the 50 nm pores inside the PC membranes, being produced by track etching, had interpore spacings that were on average much larger than the pore diameter.

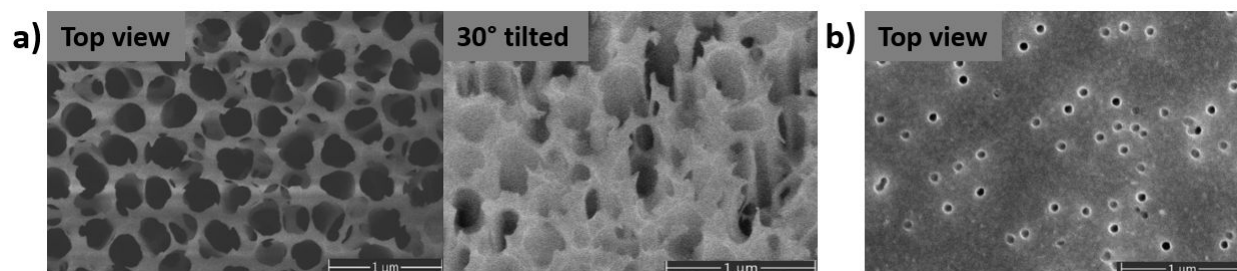


Figure 2. SEM images for two different membrane samples filled with cobalt nanowires. a) 200 nm AAO membrane sample under high vacuum (top view and 30° tilted with respect to the top view). b) 50 nm PC membrane sample under a 100 Pa vapor pressure atmosphere.

XRD. The XRD patterns of the two 200 nm samples grown in AAO membranes (with and without additives) are represented in Figure 3.

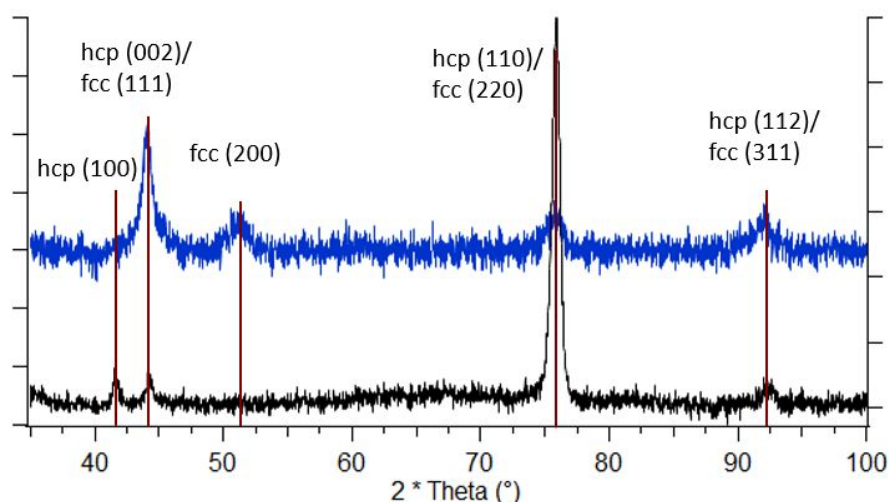


Figure 3. XRD patterns collected on 200 nm Co nanowires grown in AAO membranes (top/blue: with; bottom/black: without organic additives). The samples are analyzed with the membrane plane being in the XRD diffraction plane.

There have been numerous studies in the literature discussing the correlation between additive use and sample microstructure.^{46–48} Here, all the observed peaks in the diffraction pattern are from cobalt, either in the *fcc* or *hcp* phase. Three peaks are observed around 44.3°, 75.9° and 92.4°, which can be assigned to either *fcc* or *hcp*, irrespective of the presence of organic additives in the electrolyte during electrodeposition or not. In the reference files, the theoretical

positions of the cobalt *fcc* (111) and *hcp* (002) reflections are 44.2° and 44.8° , respectively, suggesting that the 44.3° peak mainly came from *fcc* Co. Nevertheless, even a significant contribution to this peak from *hcp* Co cannot be excluded. Besides these three peaks, a fourth peak around 51.5° is observed in the diffraction pattern of the sample synthesized with additives and can unambiguously be assigned to *fcc* Co (200). While this peak is not present for the sample without additives, another peak at 41.6° is observed that corresponded this time unambiguously to *hcp* Co (100). These observations suggest that the additives changed the main crystalline form of the wire from *hcp* to *fcc*-rich. Further useful information could also be drawn about the crystal orientation with respect to the wire axis, as exposed earlier when describing the XRD setup (Figure 1). This is particularly interesting in the case of *hcp* cobalt in order to determine the relative orientation of the *c*-axis with respect to the wire axis because the *c*-axis is the magnetic easy-axis of *hcp* Co. The *hcp* Co parts of the samples without organic additives were oriented with the *c*-axis mainly perpendicular to the wire axis since the relative intensity of the peaks corresponding to *hcp* Co (110) vs. *hcp* Co (002) is significantly higher than in polycrystalline samples.

When comparing the FWHM of the reflections of the 200 nm samples electrodeposited with and without additives, it can be seen that the reflections obtained from the former were broader than the ones obtained from the latter, indicating a smaller crystallite size due to the presence of the additives during electrodeposition. The crystallite size in both samples was estimated using Scherrer's formula based on the FWHM of the peaks in the corresponding diffractograms in Figure 3 (more details about Scherrer's formula can be found in the Supporting Information). As most of the peaks are potentially composed of two overlapping peaks corresponding to *hcp* and *fcc* Co, only the peaks around 51.5° (*fcc* Co (200)) and 41.6° (*hcp* Co (100)) can be considered when estimating the crystallite size inside the sample synthesized without and with additives, respectively. The FWHM of the peak observed at 51.5° is around 1.9° , indicating a crystallite size of around 5 nm for the sample synthesized with additives. It is noteworthy that the other peaks in the corresponding diffractogram are all thinner than this peak, therefore the average crystallite size of 5 nm was a lower limit. When analyzing the diffractogram of the sample synthesized without additives, it can be seen that the FWHM of the peak observed at 41.6° is around 0.42° , indicating a crystallite size of around 24 nm in this sample. In this case, all the other peaks in the corresponding diffractogram are broader than this peak, meaning that the

average crystallite size of the sample might be smaller than 24 nm, but the potential overlap of different peaks does not allow a precise crystallite size determination.

The XRD spectrum of the 50 nm PC membrane sample can be found in the Supporting Information (Figure S1). Unfortunately, the reflections from the gold electrode still attached to the membrane masked those from cobalt and consequently, no conclusions could be drawn regarding the crystalline structure and the average crystallite size of this sample.

Magnetic hysteresis measurement. The magnetic properties of the wires were studied at room temperature with a magnetic field applied perpendicularly (\perp) or parallel (\parallel) to the wire axis, as shown in Figure 4 and S3.

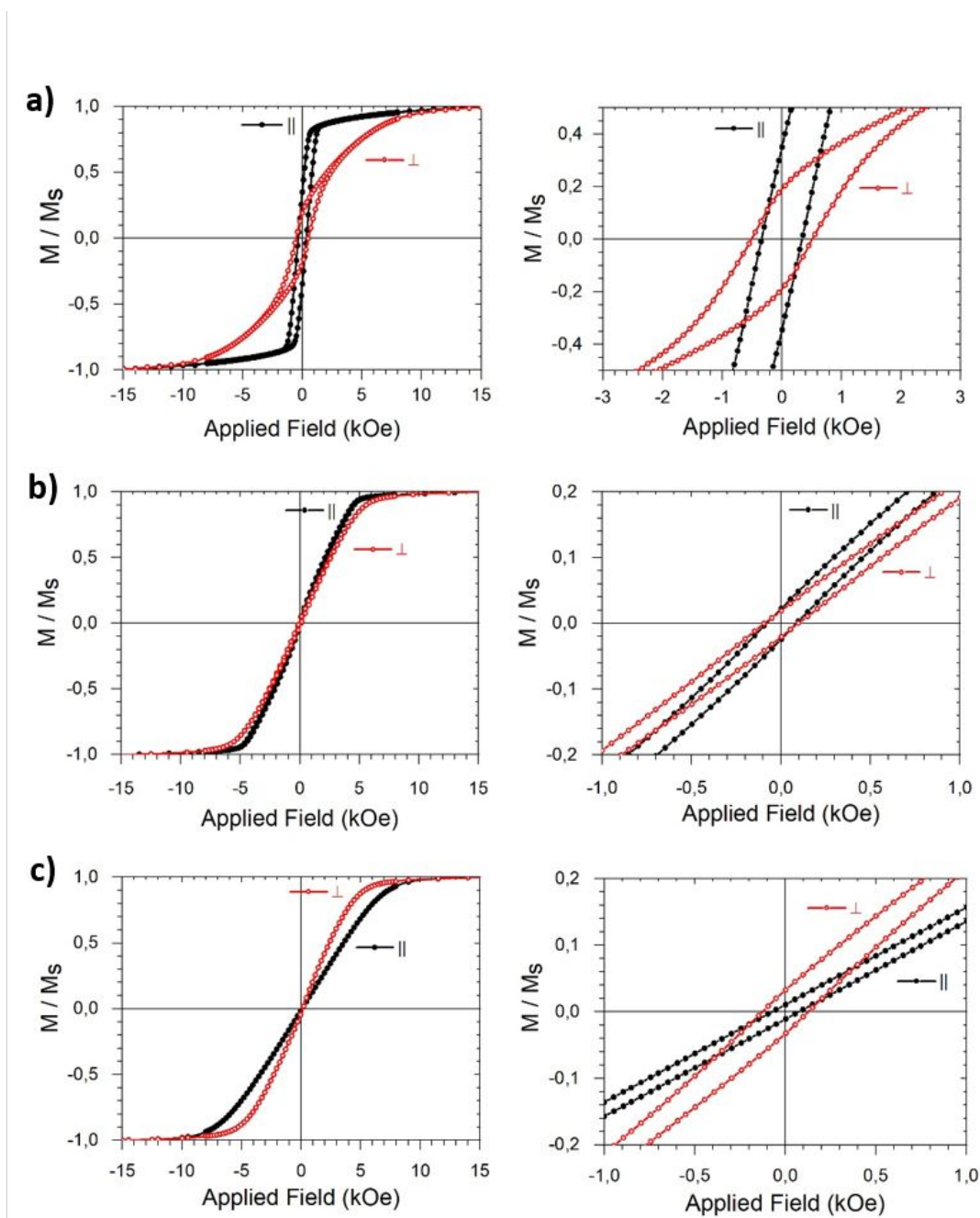


Figure 4. Magnetic hysteresis loops recorded at ambient temperature with the field applied perpendicular (\perp , red hollow symbols) or parallel (||, black full symbols) to the cobalt wires. a) 50 nm Co nanowires grown in a PC membrane with additives, b) 200 nm Co nanowires grown in

AAO membranes with additives, and c) 200 nm Co nanowires grown in AAO membranes without additives in electrolyte. The magnetic loop of the 50 nm sample grown without additives was very similar to the one with additives. For clarity, it is shown in Supporting information Figure S3. Left: full loops. Right: Zoom-in views of the full loops.

The 50 nm Co nanowires grown in a PC membrane exhibited very similar squared hysteresis loops regardless of the presence of organic additives. The coercivity of about 500 Oe when measured on-axis (i.e. parallel), was about an order of magnitude larger than that in typical Co films. This coercivity enhancement is due to the small nanowire diameter, which impedes the domain wall propagation mechanism during magnetization reversal.^{49–51} The magnetic easy axis of the wires can be determined by comparing the applied magnetic fields needed for saturation for the different directions of the applied field.

A clear magnetic easy axis parallel (positive magnetic anisotropy) to the nanowires is observed for the 50 nm sample, due to the shape anisotropy resulting from the strong saturation field ($2\pi M_S$) of 8.8 kOe required to orient the magnetization away from the wire axis (Figure 4a).²⁷ In the 200 nm Co nanowire samples grown in AAO membranes, the magnetic properties exhibited significant differences. The coercivity enhancement was reduced to values below 120 Oe, due to

the larger nanowire diameters. It is well known that a large diameter favors the formation of domain walls along the wire axis thus degrading coercivity.⁵² Wall motion occurring during magnetization reversal can be affected by several parameters such as pinning or metal-insulator stress interfaces,⁵⁰ but everything else equal, coercivity is expected, as observed here, to vary linearly with the ratio of magnetic anisotropy to magnetization.⁵³ Furthermore, when cobalt was electrodeposited in the presence of additives, i.e. *fcc*-rich according to XRD, the nanowire axis (parallel geometry) was still the magnetic easy axis. However, its difference with the perpendicular geometry was much smaller (Figure 4b), as the much closer spacing between nanowires leads to strong dipolar interaction that prefers antiferromagnetic alignment.^{10,54,55} In contrast, the *hcp*-rich 200 nm sample, synthesized without additives, exhibited a magnetic easy axis perpendicular to the wire axis (negative magnetic anisotropy) (Figure 4c). This is a manifestation of the *hcp* *c*-axis being perpendicular to the nanowires^{56,57}, as suggested by the XRD diffraction patterns of Figure 3.

Internal field NMR. In metallic cobalt structures, valuable information may be obtained from the IF NMR spectrum, such as the crystalline and magnetic structure. Although not as commonly used as XRD or magnetometry, it nicely complements these methods due to its very local

(nanoscale) character. The general spectral features of IF NMR in *fcc* or *hcp* cobalt nanostructures are as follows. At room temperature, the peak around 213 MHz can be assigned to signal coming from ^{59}Co nuclei in *fcc* multidomain structures.^{30,32} By symmetry of the *fcc* structure, this peak is generally narrow and well defined. A small peak around 216 MHz can be distinguished, which is in the literature sometimes assigned to Co in a single-domain magnetic structures, with the difference compared to the multidomain *fcc* being due to the demagnetizing field effect.^{32,58} However, this peak assignment is generally done when analyzing Co nanoparticles and not for oriented systems like nanowires. In nanowires the form factor is not the same one as in spheres⁵⁹ and consequently the demagnetizing field would lead to a different frequency shift in single-domain *fcc*. Possible origins of this peak could therefore be *fcc* stacking faults with a higher internal field compared to pure *fcc*^{60,61} or *fcc* structures with a residual demagnetizing field. The signal coming from anisotropic *hcp* structures is generally much broader than the one corresponding to *fcc*. A broad peak between 217 MHz and 222 MHz is often assigned to *hcp* cobalt without distinction between signal arising from mono- and multidomain structures.^{32,62,63} Additional information about the magnetic structure can be obtained from the variation of the optimal power with frequency, which is inversely proportional

to the enhancement factor. As the enhancement is much stronger for nuclei situated inside a domain-wall structure than for those inside the domain itself, less power is needed for the optimal excitation of the former.^{43,44,62} In a similar fashion, the signal arising from ^{59}Co nuclei inside domain walls will also be enhanced much more than from the ones inside the domains, which means that the main signal observed when analyzing multidomain structures will be from the excitation of the domain walls and not from the domains.^{43,64}

Figure 5 displays the IF NMR spectra in the frequency range associated with ^{59}Co resonances. For all samples, the spectral features were similar and supported the conclusion that both *hcp* and *fcc* structures coexisted (Figure 5a-c). While the XRD analysis suggests the presence of *fcc* or *hcp*-rich structures in the 200 nm samples, depending on the presence of additives in the electrolyte during the wire deposition or not, this difference was not apparent by NMR.

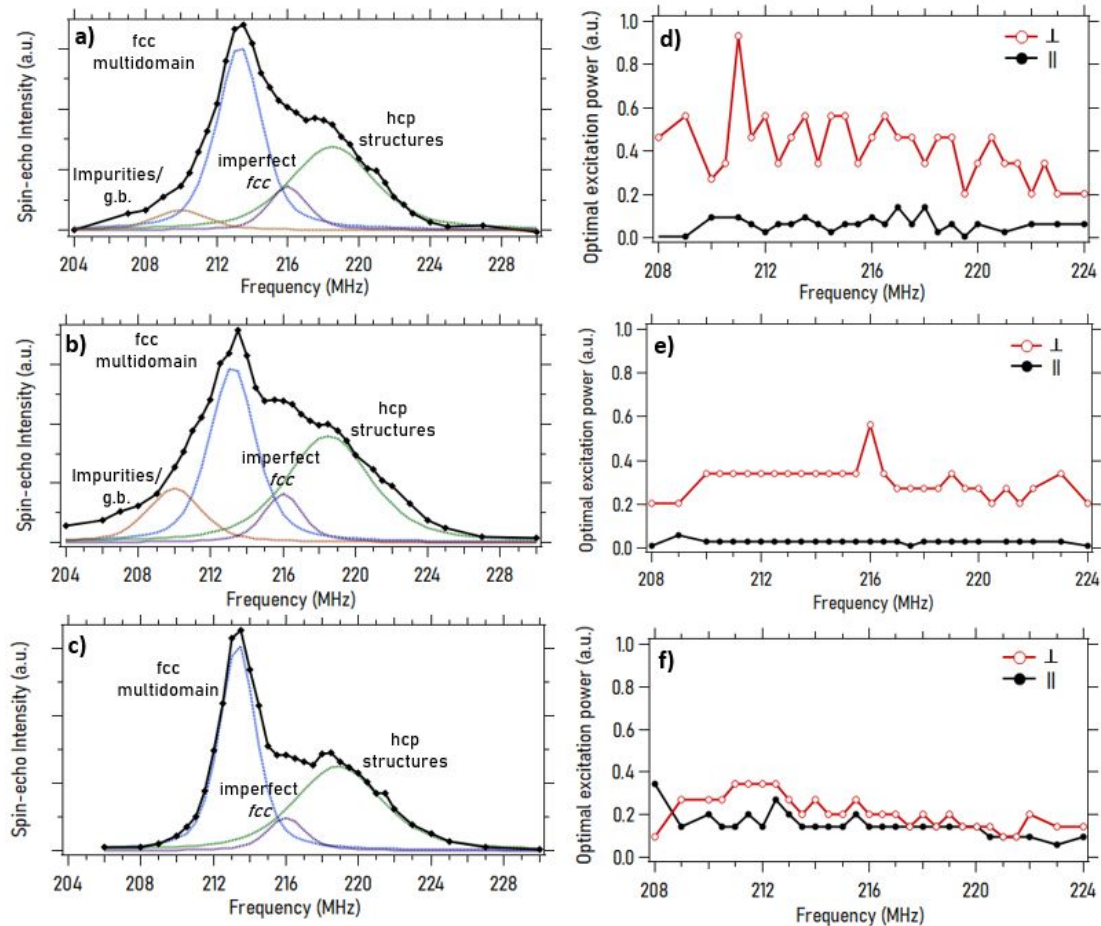


Figure 5. ^{59}Co IF NMR room temperature spectra: a) 50 nm Co nanowires grown in PC membrane, b) 200 nm Co nanowires grown in AAO membranes with organic additives (XRD *fcc*-rich), and c) 200 nm Co nanowires grown in AAO membranes without organic additives (XRD *hcp*-rich). A tentative decomposition into peaks corresponding to different crystalline and magnetic structures is also presented (g.b. = grain boundaries). The spectral shape is identical regardless of the orientation between the *rf* pulse and the wire axis, so only one orientation is represented here. The numerical comparison of the decomposition and the corresponding fitting

parameters can be found in the Supporting Information (Figure S5, Table S4). The graphs d), e) and f) correspond to the optimal excitation power for each of the left-side graphs for different orientations: The red line (hollow spheres) corresponds to a perpendicular (\perp) orientation between the direction of the rf pulse and the wire axis, the black line (full spheres) to a parallel (\parallel) one.

Indeed, in all cases, a significant resonance in the 217-222 MHz range together with a peak around 213 MHz revealed the presence of both *hcp* and *fcc* components, with similar weights for both samples (The comparison of the weights in the decomposition can be found in the Supporting Information (Figure S5)). The distribution of the optimal power, and hence of the enhancement factor, was constant over the whole spectrum range for all studied samples (Figure 5d-f). No distinction in that respect could be made between the 213 MHz resonance of the *fcc* multidomain structures and the rest of the spectra. One could thus conclude that most of the signal in the spectrum, also in the *hcp* Co part, arose from the excitation of the walls in multidomain structures, establishing that the magnetic structure of the nanowires was broken up into magnetic domains. The signal was dominated by the excitation of the domain walls.^{43,64} A significant difference between the spectra obtained from samples synthesized in presence (Figure

5a-b) and in absence (Figure 5c) of organic additives is the occurrence of a signal at frequencies below the main peak for the samples synthesized with additives. Such a signal is usually attributed to arise from grain boundaries, impurities or interfaces^{61,65} and can be fitted quite well with one peak around 210 MHz in the present spectra.

Experiments with different radio frequency (*rf*) field orientations relative to the wire axis have been performed, but the shape of the resulting spectra was identical for both orientations for all analyzed samples. However, a change in the power needed for an optimal excitation could be observed for some samples. For the samples for which the VSM measurements revealed a magnetic easy axis parallel to the wire axis (50 nm Co wires & 200 nm wires grown with additive), the enhancement factor (inversely related to the optimal power) was stronger for the *rf* field *parallel* to the wire axis than for the *perpendicular* orientation (Figure 5d-e). In contrast, the 200 nm Co wires grown without additives, for which VSM revealed an easy axis perpendicular to the wire axis, had a similar enhancement factor for both orientations (Figure 5f). These results provided more information on the magnetic domain structure, as will be discussed in the following section.

4. DISCUSSIONS

From XRD and magnetometry measurements, it was apparent that the samples had different crystalline and therefore magnetic structures. Concerning the crystalline structure, XRD suggested that the 200 nm nanowires produced with organic additives had an enriched *fcc* structure, while the 200 nm nanowires produced without organic additives had a *hcp*-rich structure with a *c*-axis perpendicular to the wire axis. However, due to the oriented character of the sample during the XRD experiments and the overlapping of the main *fcc* and *hcp* Co peaks, a quantitative phase determination was not unambiguously possible. In addition, XRD experiments only detect signal coming from relatively large cobalt coherent domains, while NMR is sensible to the whole sample. Indeed, the IF NMR spectra revealed that, at the nanoscale, both crystalline structures were present in more or less the same relative amount.

Concerning the magnetic structures, magnetometry and IF NMR results supported each other. The $M(H)$ hysteretic behavior has already been observed in previous articles analyzing cobalt wires of different diameters inside track-etched polymer membranes.^{10,27,34} The physical basis for the observed magnetic anisotropy of soft ferromagnetic materials is well known.⁶⁶ It results from the superposition of shape anisotropy, magnetocrystalline anisotropy and wire-wire interactions

(see for example the discussions of magnetic anisotropy in Co nanowires in references ^{27,34}).

Since the nanowire shape anisotropy favors a magnetization alongside the wire axis, this is the preferred configuration for wires with a weakly anisotropic crystalline structure, like *fcc* cobalt.

On the other hand, a strong crystalline anisotropy (like *hcp* Co) perpendicular to the wire axis will be in competition with the shape anisotropy, possibly leading to a magnetic easy axis perpendicular to the wires.^{56,57,67,68}

The case of the Co nanowires with a relatively narrow diameter of 50 nm grown in a PC membrane was the most straightforward as it was dominated by shape anisotropy. In this instance, the dipolar field acting on a wire due to its neighbors can safely be neglected because of the large interwire distances. Furthermore, the small 50 nm diameter, combined with the μm -scale wire length, resulted in a strong shape anisotropy^{27,34}, as reflected in the saturation field difference of the sample (Figure 4a). It could be inferred that at zero field, the magnetic structure, confined by the wire diameter, was broken up into magnetic domains with on-axis remanent magnetic moments. This conclusion was strongly supported by the anisotropy of the IF NMR enhancement factor as function of the orientation of the wire axis to the excitation field (Figure 5d). It must be recalled that the flat frequency dispersion of the enhancement factor

established that the IF NMR signal of our samples arose predominantly from the excitation of domain walls. In this case, the enhancement factor finds its origin in the periodic displacement of the domain walls under the effect of the *rf* field, a displacement which is favored when the field is oriented along the domain magnetization⁴³, as represented schematically in Figure 6a. *Rf* fields with a different orientation compared to the domain axes will displace the walls less efficiently.⁶⁹ Consequently, the higher enhancement recorded when the *rf* field was applied on axis with the nanowires supported the conclusions that the magnetic domains were magnetized along the wires. Note that the same experiments have been performed on 50 nm wires deposited without the presence of organic additives in the electrolyte, leading to the same results regarding the magnetic anisotropy (Supporting Information Figure S3 & S4). In contrast, the magnetic properties of the 200 nm samples strongly depended on the synthesis conditions, indicating that the magnetic behavior of the 50 nm wires is controlled indeed by the shape anisotropy.

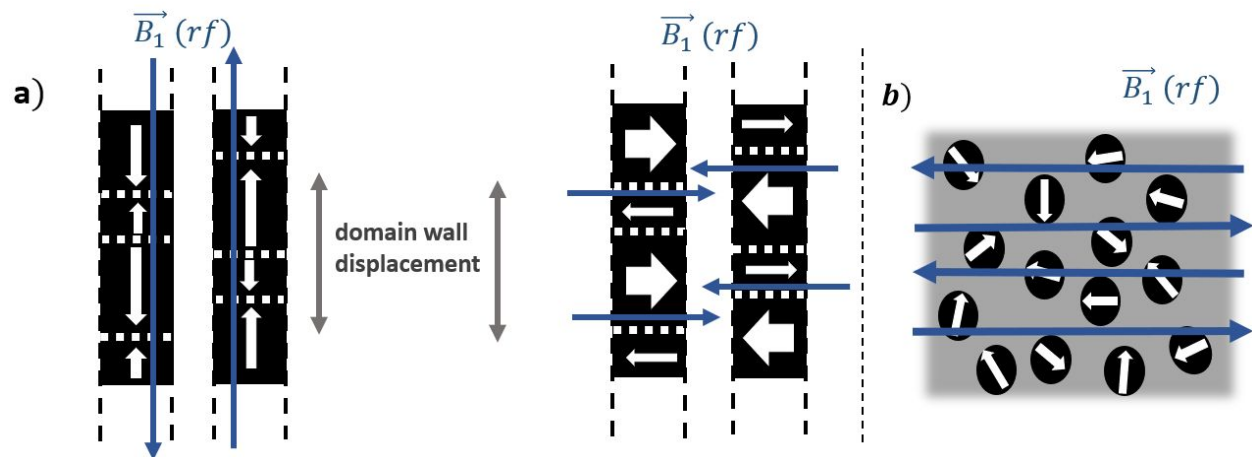


Figure 6. a) Orientation of the optimal excitation field as function of the domain wall structure.

A rf field (B_1) with this orientation will efficiently displace the domain walls back and forth by favoring the growth of domains, as shown schematically. Left: domains alongside the wire axis: 50 nm & 200 nm nanowires with additives. Right: domains perpendicular to the wire axis: 200 nm without additives. b) Random orientations of the in-plane magnetic domains for the sample without additives, which are therefore more or less aligned with the orientation of the rf field perpendicular to the wire axis.

For the two samples of 200 nm Co nanowires grown in AAO membranes, the same analysis could be performed. For the sample electrodeposited in presence of additives in the electrolyte,

the enhancement factor was higher for a rf field orientation along the wire axis (Figure 5e), consistent with the magnetic easy axis along the nanowires detected by VSM (Figure 4b). In contrast, for the 200 nm sample electrodeposited without additives, VSM revealed a magnetic easy axis perpendicular to the nanowires (Figure 4c), while the enhancement factor did not reveal any strong anisotropy (Figure 5f).

These observations raised two questions. First, why did the latter sample show no anisotropy of the IF NMR enhancement factor? Actually, this apparent contradiction can be explained on simple geometrical considerations. While the c -axis of the hcp crystallites (easy magnetic axis) was preferentially oriented perpendicular to the wire axis, its azimuthal angle was evenly distributed because of the axial symmetry of the wires, as already observed by magnetic torque measurements.^{27,67} As represented in the membrane top view of Figure 6b, even when the rf field was perpendicular to the wire axis, it could not coincide with all possible the orientations of the magnetic domains. As a result, the enhancement factor had an intermediate value between the one for a perpendicular and a parallel orientation. Due to angular symmetry, the overall enhancement factor can be approximated by:

$$\eta_{mean} = \frac{2}{\pi} * \int_0^{\frac{\pi}{2}} \eta(\theta) d\theta$$

with θ the angle between the domain orientation and the rf field. Approximations of the expression of the enhancement factor as function of θ , $\eta(\theta)$, have been proposed by Stearns et al.⁶⁹. The power needed for an optimal excitation was therefore intermediate between the one needed for a perpendicular and a parallel orientation between the excitation field and the domain direction, observed for the samples with organic additives. Nevertheless, this reduced enhancement factor for experiments with a *perpendicular* orientation still does not fully explain why it is the same as for experiments performed with a *parallel* orientation. In the case of a parallel orientation between the wire and rf field, the rf field would be perpendicular to all the domains normal to the wire axis, independently of their azimuthal angle, resulting in an even lower enhancement. An additional explanation is the fact that the wires were composed of a mixture of *hcp* and *fcc* Co crystalline structures, as deduced from the IF NMR spectrum (Figure 5c). Due to competition between the shape anisotropy and the perpendicular crystalline anisotropy (only from the *hcp* Co phases), the overall easy magnetic axis perpendicular to the wire was not very strong. This led to a situation with mixed domain orientations, where, besides

their predominant perpendicular orientation, a significant part of the domains was also oriented alongside the wire axis.

Second, what is the origin of the different magnetic behaviors of the two samples of 200 nm Co nanowires grown in AAO membranes? This can be discussed in terms of competition between shape and magnetocrystalline anisotropy, as well as the effect of dipolar interactions. From geometrical considerations, the shape anisotropy was reduced and the dipolar interactions increased in the 200 nm samples compared to the 50 nm one. As a result, the magnetic easy axis was distributed more off axis, the coercivity, the remanence and the effective magnetic energy were reduced. As both samples had the same geometrical configuration, the different magnetic behavior must originate from a variation in their crystalline anisotropy. The XRD results (shown in Figure 3) suggested a first explanation: The sample grown in presence of additives appeared to be *fcc*-rich, resulting in a low crystalline anisotropy and a magnetic easy axis alongside the wire due to the effect of the shape anisotropy. The sample grown in absence of additives on the other hand, appeared to be *hcp*-rich with a *c*-axis perpendicular to the wire axis, leading to a strong crystalline anisotropy and magnetic easy axis perpendicular to the wire. The analysis of the IF NMR spectra proposes an alternative explanation, however, as it shows an almost equal

distribution of cobalt atoms between *fcc* and *hcp* crystallites for all the samples studied (Figure 5a-c). Nevertheless, a significant difference between the IF NMR spectra of the samples is that the ^{59}Co resonances of the 200 nm sample without additives were sharper, in particular with no extension towards the 210 MHz frequency range. Signal from such a low frequency range is generally attributed to grain boundaries, impurities or interfaces^{61,65} From IF NMR this sample appeared thus more crystallized than the two others deposited with additives. When studying the deposition of cobalt thin films under similar conditions, it has been observed that the addition of organic additives, such as PEG, tends to inhibit the crystalline growth,^{70,71} while in cobalt nanowires crystallite size is known to impact magnetic anisotropy and coercivity.^{72,73} As a result, in our samples the size of the cobalt crystallites decreases, as reflected in the broader XRD and NMR peak width. In addition more grain boundaries are created and organic impurities from the additives, such as sulfur, tend to be incorporated inside the structure⁷¹, explaining the additional NMR peak at lower frequencies. Besides differences in crystal symmetry (*fcc* or *hcp*), for the cobalt nanowires under consideration a crucial structural parameter to control magnetic anisotropy appeared to be differences in the crystallite size and grain boundaries.

5. CONCLUSIONS

Despite being easy to perform on a standard commercial solid-state NMR spectrometer, IF NMR is not a widespread method to characterize cobalt magnetic structures. While concerning the magnetic structure, magnetometry and IF NMR provided essentially the same information regarding anisotropy, concerning the crystalline structure, IF NMR nicely complemented XRD characterization. Indeed, in our study of cobalt nanowires, it provided a more accurate picture of the distribution of *fcc* and *hcp* domains as well as of the presence and influence of defects at coherent domain boundaries. This allowed to better understand the influence of the presence of additives during the electrodeposition of cobalt on the magnetic properties of the formed nanowires. It was established that the organic additives determine the magnetic anisotropy of the nanowires more through the control of the grain boundaries than by modifying the *fcc* / *hcp* balance.

ASSOCIATED CONTENT

Supporting Information.

The following files are available free of charge. Supplementary XRD and IF NMR results, characterization of the 50 nm sample deposited in absence of polymer additives (PDF).

AUTHOR INFORMATION

Corresponding Author

Jean-Baptiste d'Espinose de Lacaillerie - SIMM, ESPCI Paris, Université PSL, CNRS UMR

7615, 10 Rue Vauquelin, 75005, Paris, France ; [orcid.org/ 0000-0002-2463-6877](https://orcid.org/0000-0002-2463-6877) ;

Email: jean-baptiste.despinose@espci.fr

Present Addresses

† Alberto Quintana's present address - Institut de Ciència de Materials de Barcelona, Barcelona, Catalunya, Spain.

Author Contributions

The manuscript was written through contributions of all authors. All authors have given approval to the final version of the manuscript. IF NMR, XRD and SEM experiments were performed an

analyzed by the ESPCI Paris team. Samples were synthesized by the GU team which also performed the magnetometry measurements.

ACKNOWLEDGMENT

NMR equipment at ESPCI Paris is funded in part by the Paris Region. This project has received funding from the European Union's Horizon 2020 research and innovation program under the Marie Skłodowska-Curie grant agreement No 754387. Work at Georgetown University has been supported by the US NSF (ECCS-1933527). The acquisition of a Magnetic Property Measurements System (MPMS3) at GU, which was used in this investigation, was supported by the US-NSF (DMR-1828420). Bruno Bresson (ESPCI) is thanked for performing the SEM analysis.

REFERENCES

- (1) Staño, M.; Fruchart, O. Magnetic Nanowires and Nanotubes. In *Handbook of Magnetic Materials*; Elsevier, 2018; Vol. 27, pp 155–267. <https://doi.org/10.1016/bs.hmm.2018.08.002>.
- (2) Vazquez, M. Cylindrical Nanowire Arrays: From Advanced Fabrication to Static and Microwave Magnetic Properties. *J. Magn. Magn. Mater.* **2022**, *543*, 168634. <https://doi.org/10.1016/j.jmmm.2021.168634>.
- (3) Fert, A.; Piraux, L. Magnetic Nanowires. *J. Magn. Magn. Mater.* **1999**, *200* (1–3), 338–358. [https://doi.org/10.1016/S0304-8853\(99\)00375-3](https://doi.org/10.1016/S0304-8853(99)00375-3).
- (4) Blondel, A.; Meier, J. P.; Doudin, B.; Ansermet, J. -Ph. Giant Magnetoresistance of Nanowires of Multilayers. *Appl. Phys. Lett.* **1994**, *65* (23), 3019–3021. <https://doi.org/10.1063/1.112495>.
- (5) Liu, K.; Nagodawithana, K.; Searson, P. C.; Chien, C. L. Perpendicular Giant Magnetoresistance of Multilayered Co/Cu Nanowires. *Phys. Rev. B* **1995**, *51* (11), 7381–7384. <https://doi.org/10.1103/PhysRevB.51.7381>.
- (6) Maurice, J.-L.; Imhoff, D.; Etienne, P.; Durand, O.; Dubois, S.; Piraux, L.; George, J.-M.; Galtier, P.; Fert, A. Microstructure of Magnetic Metallic Superlattices Grown by Electrodeposition in Membrane Nanopores. *J. Magn. Magn. Mater.* **1998**, *184* (1), 1–18. [https://doi.org/10.1016/S0304-8853\(97\)01104-9](https://doi.org/10.1016/S0304-8853(97)01104-9).
- (7) Wong, J.; Greene, P.; Dumas, R. K.; Liu, K. Probing Magnetic Configurations in Co/Cu Multilayered Nanowires. *Appl. Phys. Lett.* **2009**, *94* (3), 032504. <https://doi.org/10.1063/1.3073740>.
- (8) Berganza, E.; Marqués-Marchán, J.; Bran, C.; Vazquez, M.; Asenjo, A.; Jaafar, M. Evidence of Skyrmion-Tube Mediated Magnetization Reversal in Modulated Nanowires. *Materials* **2021**, *14* (19), 5671. <https://doi.org/10.3390/ma14195671>.
- (9) Fernández-Pacheco, A.; Streubel, R.; Fruchart, O.; Hertel, R.; Fischer, P.; Cowburn, R. P. Three-Dimensional Nanomagnetism. *Nat. Commun.* **2017**, *8* (1), 15756. <https://doi.org/10.1038/ncomms15756>.
- (10) Burks, E. C.; Gilbert, D. A.; Murray, P. D.; Flores, C.; Felter, T. E.; Charnvanichborikarn, S.; Kucheyev, S. O.; Colvin, J. D.; Yin, G.; Liu, K. 3D Nanomagnetism in Low Density

- Interconnected Nanowire Networks. *Nano Lett.* **2021**, *21* (1), 716–722. <https://doi.org/10.1021/acs.nanolett.0c04366>.
- (11) Lee, S. A.; Yang, J. W.; Choi, S.; Jang, H. W. Nanoscale Electrodeposition: Dimension Control and 3D Conformality. *Exploration* **2021**, *1* (3), 20210012. <https://doi.org/10.1002/EXP.20210012>.
- (12) Santhi, U.; Ngui, W. K.; Samykano, M.; Sudhakar, K.; Kadirgama, K.; Sangmesh, B.; Kumar, M. A. R. Cobalt Nanowires: Advancing into Future Nanomaterial. In *AIP Conference Proceedings*; Kuantan, Malaysia, 2019; p 020006. <https://doi.org/10.1063/1.5085949>.
- (13) Déjardin, J.-L.; Franco, A.; Vernay, F.; Kachkachi, H. Ferromagnetic Resonance of a Two-Dimensional Array of Nanomagnets: Effects of Surface Anisotropy and Dipolar Interactions. *Phys. Rev. B* **2018**, *97* (22), 224407. <https://doi.org/10.1103/PhysRevB.97.224407>.
- (14) Zhang, H.; Jia, W.; Sun, H.; Guo, L.; Sun, J. Growth Mechanism and Magnetic Properties of Co Nanowire Arrays by AC Electrodeposition. *J. Magn. Magn. Mater.* **2018**, *468*, 188–192. <https://doi.org/10.1016/j.jmmm.2018.08.013>.
- (15) Das, B.; Mandal, K.; Sen, P.; Bakshi, A.; Das, P. Directional Change of Magnetic Easy Axis of Arrays of Cobalt Nanowires: Role of Non-Dipolar Magnetostatic Interaction. *Phys. B Condens. Matter* **2012**, *407* (18), 3767–3773. <https://doi.org/10.1016/j.physb.2012.05.058>.
- (16) Chen, W.-H.; Cheng, H.-C.; Hsu, Y.-C.; Uang, R.-H.; Hsu, J.-S. Mechanical Material Characterization of Co Nanowires and Their Nanocomposite. *Compos. Sci. Technol.* **2008**, *68* (15–16), 3388–3395. <https://doi.org/10.1016/j.compscitech.2008.09.030>.
- (17) Hayashi, M.; Thomas, L.; Rettner, C.; Moriya, R.; Parkin, S. S. P. Real Time Observation of the Field Driven Periodic Transformation of Domain Walls in Permalloy Nanowires at the Larmor Frequency and Its First Harmonic. *Appl. Phys. Lett.* **2008**, *92* (11), 112510. <https://doi.org/10.1063/1.2890036>.
- (18) Parkin, S. S. P.; Hayashi, M.; Thomas, L. Magnetic Domain-Wall Racetrack Memory. *Science* **2008**, *320* (5873), 190. <https://doi.org/10.1126/science.1145799>.
- (19) Herrera Diez, L.; Liu, Y. T.; Gilbert, D. A.; Belmeguenai, M.; Vogel, J.; Pizzini, S.; Martinez, E.; Lamperti, A.; Mohammedi, J. B.; Laborieux, A.; Roussigné, Y.; Grutter, A. J.; Arenholtz, E.; Quarterman, P.; Maranville, B.; Ono, S.; Hadri, M. S. E.; Tolley, R.;

- Fullerton, E. E.; Sanchez-Tejerina, L.; Stashkevich, A.; Chérif, S. M.; Kent, A. D.; Querlioz, D.; Langer, J.; Ocker, B.; Ravelosona, D. Nonvolatile Ionic Modification of the Dzyaloshinskii-Moriya Interaction. *Phys. Rev. Appl.* **2019**, *12* (3), 034005. <https://doi.org/10.1103/PhysRevApplied.12.034005>.
- (20) Parkin, S.; Yang, S.-H. Memory on the Racetrack. *Nat. Nanotechnol.* **2015**, *10* (3), 195–198. <https://doi.org/10.1038/nnano.2015.41>.
- (21) Kac, M.; Zarzycki, A.; Kac, S.; Kopec, M.; Perzanowski, M.; Dutkiewicz, E. M.; Suchanek, K.; Maximenko, A.; Marszalek, M. Effect of the Template-Assisted Electrodeposition Parameters on the Structure and Magnetic Properties of Co Nanowire Arrays. *Mater. Sci. Eng. B* **2016**, *211*, 75–84. <https://doi.org/10.1016/j.mseb.2016.06.004>.
- (22) Caffarena, V. R.; Guimarães, A. P.; Folly, W. S. D.; Silva, E. M.; Capitaneo, J. L. Magnetic Behavior of Electrodeposited Cobalt Nanowires Using Different Electrolytic Bath Acidities. *Mater. Chem. Phys.* **2008**, *107* (2–3), 297–304. <https://doi.org/10.1016/j.matchemphys.2007.07.016>.
- (23) Ferré, R.; Ounadjela, K.; George, J. M.; Piraux, L.; Dubois, S. Magnetization Processes in Nickel and Cobalt Electrodeposited Nanowires. *Phys. Rev. B* **1997**, *56* (21), 14066–14075. <https://doi.org/10.1103/PhysRevB.56.14066>.
- (24) Wegrowe, J.-E.; Kelly, D.; Franck, A.; Gilbert, S. E.; Ansermet, J.-Ph. Magnetoresistance of Ferromagnetic Nanowires. *Phys. Rev. Lett.* **1999**, *82* (18), 3681–3684. <https://doi.org/10.1103/PhysRevLett.82.3681>.
- (25) Piraux, L.; Dubois, S.; Ferain, E.; Legras, R.; Ounadjela, K.; George, J. M.; Maurice, J. L.; Fert, A. Anisotropic Transport and Magnetic Properties of Arrays of Sub-Micron Wires. *J. Magn. Magn. Mater.* **1997**, *165* (1–3), 352–355. [https://doi.org/10.1016/S0304-8853\(96\)00553-7](https://doi.org/10.1016/S0304-8853(96)00553-7).
- (26) Wernsdorfer, W.; Doudin, B.; Mailly, D.; Hasselbach, K.; Benoit, A.; Meier, J.; Ansermet, J.-Ph.; Barbara, B. Nucleation of Magnetization Reversal in Individual Nanosized Nickel Wires. *Phys. Rev. Lett.* **1996**, *77* (9), 1873–1876. <https://doi.org/10.1103/PhysRevLett.77.1873>.
- (27) Henry, Y.; Ounadjela, K.; Piraux, L.; Dubois, S.; George, J.-M.; Duvail, J.-L. Magnetic Anisotropy and Domain Patterns in Electrodeposited Cobalt Nanowires. *Eur. Phys. J. B* **2001**, *20* (1), 35–54. <https://doi.org/10.1007/s100510170283>.

- (28) Chen, G.; Mascaraque, A.; Jia, H.; Zimmermann, B.; Robertson, M.; Conte, R. L.; Hoffmann, M.; González Barrio, M. A.; Ding, H.; Wiesendanger, R.; Michel, E. G.; Blügel, S.; Schmid, A. K.; Liu, K. Large Dzyaloshinskii-Moriya Interaction Induced by Chemisorbed Oxygen on a Ferromagnet Surface. *Sci. Adv.* **2020**, *6* (33), eaba4924. <https://doi.org/10.1126/sciadv.aba4924>.
- (29) Chen, G.; Robertson, M.; Hoffmann, M.; Ophus, C.; Fernandes Cauduro, A. L.; Lo Conte, R.; Ding, H.; Wiesendanger, R.; Blügel, S.; Schmid, A. K.; Liu, K. Observation of Hydrogen-Induced Dzyaloshinskii-Moriya Interaction and Reversible Switching of Magnetic Chirality. *Phys. Rev. X* **2021**, *11* (2), 021015. <https://doi.org/10.1103/PhysRevX.11.021015>.
- (30) Gossard, A. C.; Portis, A. M. Observation of Nuclear Resonance in a Ferromagnet. *Phys. Rev. Lett.* **1959**, *3* (4), 164–166. <https://doi.org/10.1103/PhysRevLett.3.164>.
- (31) Liu, Y.; Luo, J.; Shin, Y.; Moldovan, S.; Ersen, O.; Hébraud, A.; Schlatter, G.; Pham-Huu, C.; Meny, C. Sampling the Structure and Chemical Order in Assemblies of Ferromagnetic Nanoparticles by Nuclear Magnetic Resonance. *Nat. Commun.* **2016**, *7*, 11532. <https://doi.org/10.1038/ncomms11532>.
- (32) Andreev, A. S.; d’Espinose de Lacaillerie, J.-B.; Lapina, O. B.; Gerashenko, A. Thermal Stability and Hcp–Fcc Allotropic Transformation in Supported Co Metal Catalysts Probed near Operando by Ferromagnetic NMR. *Phys. Chem. Chem. Phys.* **2015**, *17* (22), 14598–14604. <https://doi.org/10.1039/C4CP05327C>.
- (33) Yakovlev, I. V.; Yakushkin, S. S.; Kazakova, M. A.; Trukhan, S. N.; Volkova, Z. N.; Gerashchenko, A. P.; Andreev, A. S.; Ishchenko, A. V.; Martyanov, O. N.; Lapina, O. B.; d’Espinose de Lacaillerie, J.-B. Superparamagnetic Behaviour of Metallic Co Nanoparticles According to Variable Temperature Magnetic Resonance. *Phys. Chem. Chem. Phys.* **2021**, *23* (4), 2723–2730. <https://doi.org/10.1039/D0CP05963C>.
- (34) Strijkers, G. J.; Dalderop, J. H. J.; Broeksteeg, M. A. A.; Swagten, H. J. M.; de Jonge, W. J. M. Structure and Magnetization of Arrays of Electrodeposited Co Wires in Anodic Alumina. *J. Appl. Phys.* **1999**, *86* (9), 5141–5145. <https://doi.org/10.1063/1.371490>.
- (35) De Riedmatten, H.; Scarani, V.; Ansermet, J.-P. Effect of Oxidation of Cobalt-Based Nanowires on NMR Spin-Lattice Relaxation. *Appl. Magn. Reson.* **2000**, *19* (3–4), 439–445. <https://doi.org/10.1007/BF03162387>.

- (36) Scarani, V.; De Riedmatten, H.; Ansermet, J.-P. ^{59}Co Nuclear Magnetic Resonance Studies of Magnetic Excitations in Ferromagnetic Nanowires. *Appl. Phys. Lett.* **2000**, *76* (7), 903–905. <https://doi.org/10.1063/1.125624>.
- (37) Scarani, V.; Doudin, B.; Ansermet, J.-P. The Microstructure of Electrodeposited Cobalt-Based Nanowires and Its Effect on Their Magnetic and Transport Properties. *J. Magn. Mater.* **1999**, *205* (2–3), 8. [https://doi.org/10.1016/S0304-8853\(99\)00513-2](https://doi.org/10.1016/S0304-8853(99)00513-2).
- (38) Doudin, B.; Wegrowe, J. E.; Gilbert, S. E.; Scarani, V.; Kelly, D.; Meier, J. P.; Ansermet, J.-P. Magnetic and Transport Properties of Electrodeposited Nanostructured Nanowires. *IEEE Trans. Magn.* **1998**, *34* (4), 968–972. <https://doi.org/10.1109/20.706328>.
- (39) Gilbert, D. A.; Burks, E. C.; Ushakov, S. V.; Abellan, P.; Arslan, I.; Felter, T. E.; Navrotsky, A.; Liu, K. Tunable Low Density Palladium Nanowire Foams. *Chem. Mater.* **2017**, *29* (22), 9814–9818. <https://doi.org/10.1021/acs.chemmater.7b03978>.
- (40) Malloy, J.; Quintana, A.; Jensen, C. J.; Liu, K. Efficient and Robust Metallic Nanowire Foams for Deep Submicrometer Particulate Filtration. *Nano Lett.* **2021**, *21* (7), 2968–2974. <https://doi.org/10.1021/acs.nanolett.1c00050>.
- (41) Vicenzo, A.; Cavallotti, P. L. Growth Modes of Electrodeposited Cobalt. *Electrochimica Acta* **2004**, *49* (24), 4079–4089. <https://doi.org/10.1016/j.electacta.2004.04.001>.
- (42) Watts, O. P. Rapid Nickel Plating. *Trans. Am. Electrochem. Soc* **1916**, *29*, 395–403.
- (43) Guimarães, A. P. *Magnetism and Magnetic Resonance in Solids*; John Wiley & Sons: New York, 1998.
- (44) Turov, E. A.; Petrov, M. P. *Nuclear Magnetic Resonance in Ferro- and Antiferromagnets*; Israel Program for scientific translations (Halsted Press): Jerusalem, 1972.
- (45) Massiot, D.; Fayon, F.; Capron, M.; King, I.; Le Calvé, S.; Alonso, B.; Durand, J.-O.; Bujoli, B.; Gan, Z.; Hoatson, G. Modelling One- and Two-Dimensional Solid-State NMR Spectra: Modelling 1D and 2D Solid-State NMR Spectra. *Magn. Reson. Chem.* **2002**, *40* (1), 70–76. <https://doi.org/10.1002/mrc.984>.
- (46) Armyanov, S. Crystallographic Structure and Magnetic Properties of Electrodeposited Cobalt and Cobalt Alloys. *Electrochimica Acta* **2000**, *45* (20), 3323–3335. [https://doi.org/10.1016/S0013-4686\(00\)00408-4](https://doi.org/10.1016/S0013-4686(00)00408-4).
- (47) Santos, J. S.; Matos, R.; Trivinho-Strixino, F.; Pereira, E. C. Effect of Temperature on Co Electrodeposition in the Presence of Boric Acid. *Electrochimica Acta* **2007**, *53* (2), 644–649. <https://doi.org/10.1016/j.electacta.2007.07.025>.

- (48) Rigsby, M. A.; Spurlin, T. A.; Reid, J. D. The Multi-Functional Role of Boric Acid in Cobalt Electrodeposition and Superfill. *J. Electrochem. Soc.* **2020**, *167* (11), 112507. <https://doi.org/10.1149/1945-7111/aba640>.
- (49) Whitney, T. M.; Searson, P. C.; Jiang, J. S.; Chien, C. L. Fabrication and Magnetic Properties of Arrays of Metallic Nanowires. *Science* **1993**, *261* (5126), 1316–1319. <https://doi.org/10.1126/science.261.5126.1316>.
- (50) Rahman, M. T.; Dumas, R. K.; Eibagi, N.; Shams, N. N.; Wu, Y.-C.; Liu, K.; Lai, C.-H. Controlling Magnetization Reversal in Co/Pt Nanostructures with Perpendicular Anisotropy. *Appl. Phys. Lett.* **2009**, *94* (4), 042507. <https://doi.org/10.1063/1.3075061>.
- (51) Liu, K.; Chien, C. L. Magnetic and Magneto-Transport Properties of Novel Nanostructured Networks. *IEEE Trans. Magn.* **1998**, *34* (4), 1021–1023. <https://doi.org/10.1109/20.706344>.
- (52) Saeki, R.; Ohgai, T. Determination of Activation Overpotential during the Nucleation of Hcp-Cobalt Nanowires Synthesized by Potentio-Static Electrochemical Reduction. *Materials* **2018**, *11* (12), 2355. <https://doi.org/10.3390/ma11122355>.
- (53) Chien, C. L. Granular Magnetic Solids (Invited). *J. Appl. Phys.* **1991**, *69* (8), 5267–5272. <https://doi.org/10.1063/1.348946>.
- (54) Kou, X.; Fan, X.; Dumas, R. K.; Lu, Q.; Zhang, Y.; Zhu, H.; Zhang, X.; Liu, K.; Xiao, J. Q. Memory Effect in Magnetic Nanowire Arrays. *Adv. Mater.* **2011**, *23* (11), 1393–1397. <https://doi.org/10.1002/adma.201003749>.
- (55) Zamani Kouhpanji, M. R.; Ghoreyshi, A.; Visscher, P. B.; Stadler, B. J. H. Facile Decoding of Quantitative Signatures from Magnetic Nanowire Arrays. *Sci. Rep.* **2020**, *10* (1), 15482. <https://doi.org/10.1038/s41598-020-72094-4>.
- (56) Chen, F.; Wang, F.; Jia, F.; Li, J.; Liu, K.; Huang, S.; Luan, Z.; Wu, D.; Chen, Y.; Zhu, J.; Peng, R.-W.; Wang, M. Periodic Magnetic Domains in Single-Crystalline Cobalt Filament Arrays. *Phys. Rev. B* **2016**, *93* (5), 054405. <https://doi.org/10.1103/PhysRevB.93.054405>.
- (57) Liu, Z.; Chang, P.-C.; Chang, C.-C.; Galaktionov, E.; Bergmann, G.; Lu, J. G. Shape Anisotropy and Magnetization Modulation in Hexagonal Cobalt Nanowires: Magnetization Modulation in Cobalt Nanowires. *Adv. Funct. Mater.* **2008**, *18* (10), 1573–1578. <https://doi.org/10.1002/adfm.200701010>.

- (58) Gossard, A. C.; Portis, A. M.; Rubinstein, M.; Lindquist, R. H. Ferromagnetic Nuclear Resonance of Single-Domain Cobalt Particles. *Phys. Rev.* **1965**, *138* (5A), A1415–A1421. <https://doi.org/10.1103/PhysRev.138.A1415>.
- (59) Osborn, J. A. Demagnetizing Factors of the General Ellipsoid. *Phys. Rev.* **1945**, *67* (11–12), 351–357. <https://doi.org/10.1103/PhysRev.67.351>.
- (60) Panissod, P. Structural and Magnetic Investigations of Ferromagnets by NMR. Application to Magnetic Metallic Multilayers. In *Frontiers in Magnetism of Reduced Dimension Systems*; Bar'yakhtar, V. G., Wigen, P. E., Lesnik, N. A., Eds.; Springer Netherlands: Dordrecht, 1998; pp 225–270. https://doi.org/10.1007/978-94-011-5004-0_10.
- (61) Sort, J.; Suriñach, S.; Muñoz, J. S.; Baró, M. D.; Wojcik, M.; Jedryka, E.; Nadolski, S.; Sheludko, N.; Nogués, J. Role of Stacking Faults in the Structural and Magnetic Properties of Ball-Milled Cobalt. *Phys. Rev. B* **2003**, *68* (1). <https://doi.org/10.1103/PhysRevB.68.014421>.
- (62) Andreev, A. S.; Lapina, O. B.; Cherepanova, S. V. A New Insight into Cobalt Metal Powder Internal Field ⁵⁹Co NMR Spectra. *Appl. Magn. Reson.* **2014**, *45* (10), 1009–1017. <https://doi.org/10.1007/s00723-014-0580-0>.
- (63) Matveev, V. V.; Baranov, D. A.; Yurkov, G. Yu.; Akatiev, N. G.; Dotsenko, I. P.; Gubin, S. P. Cobalt Nanoparticles with Preferential Hcp Structure: A Confirmation by X-Ray Diffraction and NMR. *Chem. Phys. Lett.* **2006**, *422* (4–6), 402–405. <https://doi.org/10.1016/j.cplett.2006.02.099>.
- (64) *Frontiers in Magnetism of Reduced Dimension Systems*; Bar'yakhtar, V. G., Wigen, P. E., Lesnik, N. A., Eds.; Springer Netherlands: Dordrecht, 1998. <https://doi.org/10.1007/978-94-011-5004-0>.
- (65) Cadeville, M. C.; Deportes, J. Saturation Magnetizations and High Field Susceptibilities of C and C Interstitial Solid Solutions. *Phys. Lett. A* **1972**, *41* (3), 237–238. [https://doi.org/10.1016/0375-9601\(72\)90275-7](https://doi.org/10.1016/0375-9601(72)90275-7).
- (66) Johnson, M. T.; Bloemen, P. J. H.; Broeder, F. J. A. den; Vries, J. J. de. Magnetic Anisotropy in Metallic Multilayers. *Rep. Prog. Phys.* **1996**, *59* (11), 1409–1458. <https://doi.org/10.1088/0034-4885/59/11/002>.

- (67) Ounadjela, K.; Ferré, R.; Louail, L.; George, J. M.; Maurice, J. L.; Piraux, L.; Dubois, S. Magnetization Reversal in Cobalt and Nickel Electrodeposited Nanowires. *J. Appl. Phys.* **1997**, *81* (8), 5455–5457. <https://doi.org/10.1063/1.364568>.
- (68) Prejbeanu, I. L.; Buda, L. D.; Ebels, U.; Viret, M.; Fermon, C.; Ounadjela, K. Domain Structures in Epitaxial (1010) Co Wires. *IEEE Trans. Magn.* **2001**, *37* (4), 2108–2110. <https://doi.org/10.1109/20.951068>.
- (69) Stearns, M. B. Spin-Echo and Free-Induction-Decay Measurements in Pure Fe and Fe-Rich Ferromagnetic Alloys: Domain-Wall Dynamics. *Phys. Rev.* **1967**, *162* (2), 496–509. <https://doi.org/10.1103/PhysRev.162.496>.
- (70) Ni, X.; Chen, Y.; Jin, X.; Wang, C.; Huang, Y.; Hong, Y.; Su, X.; Zhou, G.; Wang, S.; He, W.; Chen, Q. Investigation of Polyvinylpyrrolidone as an Inhibitor for Trench Super-Filling of Cobalt Electrodeposition. *J. Taiwan Inst. Chem. Eng.* **2020**, *112*, 232–239. <https://doi.org/10.1016/j.jtice.2020.06.010>.
- (71) Hu, Y.; Deb, S.; Li, D.; Huang, Q. Effects of Organic Additives on the Impurity and Grain Structure of Electrodeposited Cobalt. *Electrochimica Acta* **2021**, *368*, 137594. <https://doi.org/10.1016/j.electacta.2020.137594>.
- (72) Saini, D.; Chauhan, R. P.; Kumar, S. Effects of Annealing on Structural and Magnetic Properties of Template Synthesized Cobalt Nanowires Useful as Data Storage and Nano Devices. *J. Mater. Sci. Mater. Electron.* **2014**, *25* (1), 124–127. <https://doi.org/10.1007/s10854-013-1560-0>.
- (73) Maaz, K.; Karim, S.; Usman, M.; Mumtaz, A.; Liu, J.; Duan, J. L.; Maqbool, M. Effect of Crystallographic Texture on Magnetic Characteristics of Cobalt Nanowires. *Nanoscale Res. Lett.* **2010**, *5* (7), 1111–1117. <https://doi.org/10.1007/s11671-010-9610-5>.